Plasmon-controlled optimum gate bias for GaN heterostructure field-effect transistors



2013 Semicond. Sci. Technol. 28 055008

(http://iopscience.iop.org/0268-1242/28/5/055008)

Semicond. Sci. Technol. **28** (2013) 055008 (5pp) doi:10.1088/0268-1242/28/5/055008

# Plasmon-controlled optimum gate bias for GaN heterostructure field-effect transistors

**A Šimukovič[1], A Matulionis[1], J Liberis[1], E Šermukšnis[1], P Sakalas[1,2], F Zhang[3], J H Leach[3], V Avrutin[3] and H Morkoç[3]**

[1] Fluctuation Research Laboratory, Centre for Physical Sciences and Technology, Vilnius, LT 02300, Lithuania
[2] Chair for Electron Devices and Integrated Circuits, Technical University Dresden, Dresden, D-01062, Germany
[3] Department of Electrical and Computer Engineering, Virginia Commonwealth University, Richmond, VA 23284, USA

E-mail: simukovic@pfi.lt

Received 24 January 2013, in final form 8 March 2013
Published 9 April 2013
Online at stacks.iop.org/SST/28/055008

**Abstract**
Electron density-dependent dc, rf and power characteristics are investigated for nearly lattice-matched InAlN/AlN/GaN heterostructure field-effect transistors (HFETs). The best performance in respect to transconductance and cutoff frequency is demonstrated at the optimal gate bias of −8 V for the devices with electron sheet density of $3 \times 10^{13}$ cm$^{-2}$ (measured on Hall bars of as-grown heterostructures). The results are in fair agreement with the universal bias–density relation controlled by the plasmon-assisted ultrafast decay of nonequilibrium optical phonons launched by hot electrons.

## 1. Introduction

Wide-bandgap compound semiconductors are attractive contenders [1–4] for high-power microwave applications such as front-end low noise amplifier (LNA), featuring high reliability and survivability for power overdrive [5]. The main advantage of a heterostructure field-effect transistor (HFET) over the MESFET stems from a high-density two-dimensional electron gas (2DEG) confined in an undoped semiconductor at a heterojunction with a wide bandgap semiconductor in very close proximity to the gate metal. This feature yields excellent high-frequency performance of gallium nitride HFETs [6–8]. The main applications of GaN based HFETs are related to the power gain, especially at high frequencies [9, 10]. It would be natural to expect a higher power if more electrons were confined in the channel. A 2DEG density above $3 \times 10^{13}$ cm$^{-2}$ can be induced in the GaN channel by a lattice-matched InAlN barrier [11] and can be controlled by varying In composition in the barrier layer [12, 13]. The InAlN/GaN junction is also preferable due to high conduction band discontinuity and weak gate leakage current. Nevertheless, the electron drift velocity decreases as the 2DEG density increases because of accumulation of nonequilibrium optical phonons (hot phonons) [14]. After an experimental study of the electron drift velocity and HFET operation (cutoff frequency $f_T$, degradation and phase noise) plasmon-assisted ultrafast decay of hot phonons is resolved at a resonance 2DEG density of $(1 \pm 0.1) \times 10^{13}$ cm$^{-2}$ [15]. The resonance provides a plausible explanation for the best performance of HFETs.

This paper compares InAlN/AlN/GaN HFETs with different initial 2DEG density. The main goal is to verify and discuss the universal relation, caused by the plasmon-assisted ultrafast decay of hot phonons, between the optimal gate bias and the initial electron density.

## 2. Devices

The nominally undoped nearly lattice-matched heterostructures of $In_xAl_{1-x}N$/AlN/GaN were grown on sapphire substrates in a low-pressure custom-designed organometallic vapor phase epitaxy system. The sandwich consisted of a 250 nm AlN initiation layer, 3 $\mu$m of undoped GaN, 1 nm AlN spacer layer, 20 nm $In_xAl_{1-x}N$ barrier layer and a 2 nm GaN cap layer on the top. The In composition $x$ in the barrier layer for

 

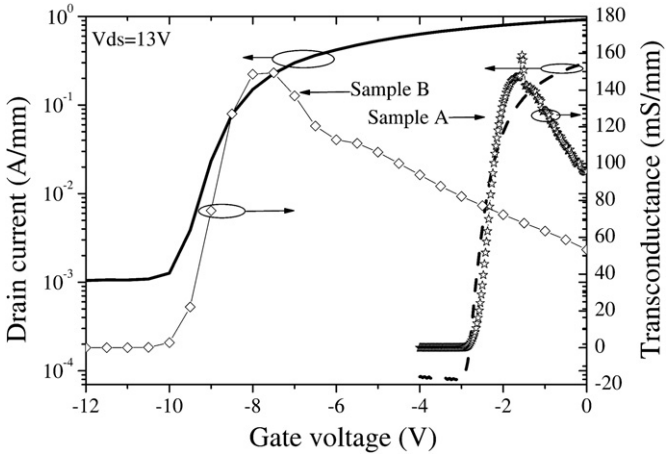


**Figure 1.** Transfer and transconductance characteristics of HFETs ($L_g = 2\ \mu$m, $W_g = 2\ \times\ 50\ \mu$m) for device A (dashed line, stars) and device B (solid line, diamonds).

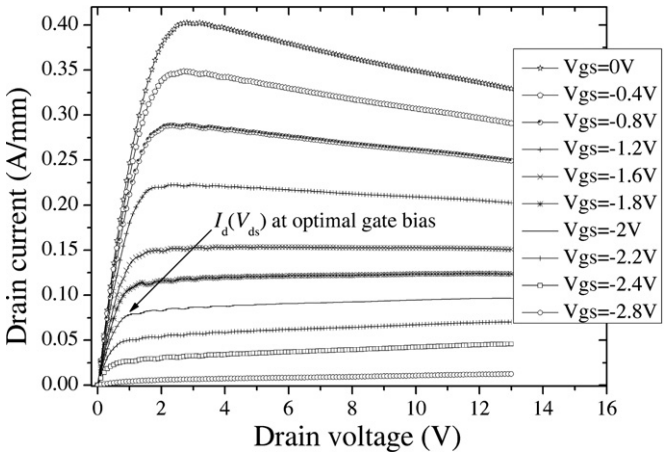


**Figure 2.** Drain current versus drain voltage of device A ($L_g = 2\ \mu$m, $W_g = 2\ \times\ 50\ \mu$m).

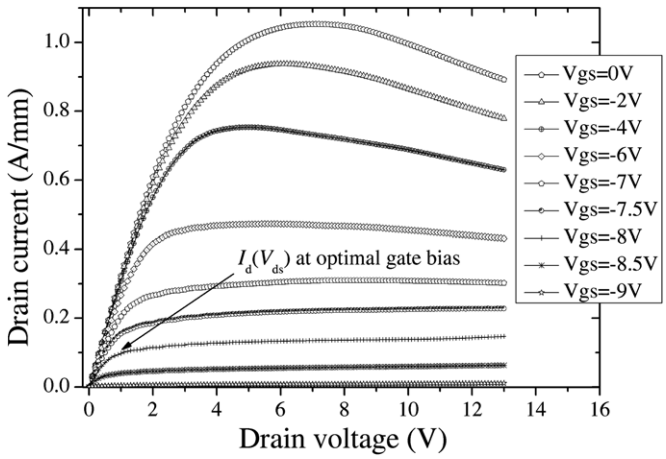


**Figure 3.** Drain current versus drain voltage of device B ($L_g = 2\ \mu$m, $W_g = 2\ \times\ 50\ \mu$m).

samples A and B was $x = 0.2$ and $x = 0.16$, respectively. Ohmic contacts for HFETs and gated Hall bars consisted of Ti/Al/Ni/Au, while Pt/Au (thickness 30/50 nm, length/width $2/2\ \times\ 50\ \mu$m) was used for the gate electrodes. The devices were mesa isolated in a SAMCO inductively coupled plasma etcher based on chlorine chemistry. The devices were not passivated. The Hall effect measurements yielded the initial 2DEG density of $n_s = 1.3\ \times\ 10^{13}$ cm$^{-2}$ and $n_s = 3\ \times\ 10^{13}$ cm$^{-2}$ for the samples A ($x = 0.2$) and B ($x = 0.16$), respectively.

## 3. Experimental setup and results

On-wafer dc (direct current) and rf (radio frequency) characteristics were measured at an ambient temperature of 25 °C with an Agilent PNA E8364B Network Analyzer, Agilent PSA E4448A Spectrum Analyzer, Agilent E5270B Precision Measurement Mainframe and Süss Microtech probestation PM8. Power measurements were carried out with a Maury Automated Tuner System ATS, including fundamental source and load tuners, Agilent E4418B Power Meter and Agilent PSG E8257D Analog Signal Generator. The *s*-parameters were measured in the frequency range from 0.25 to 26 GHz in short-open-load-thru (SOLT) calibration mode (with on-wafer impedance calibration standards). De-embedding of pad parasitics was performed using a one-step ('open' dummy) method.

The transfer characteristics for devices A and B are shown in figure 1. A higher electron density in device B supports a higher drain current $I_d$ (solid line) in saturation, compared to that (dashed line) for device A having the same geometry. More negative bias on the gate is required to pinch off the drain current if the initial 2DEG density is higher. Thus, device B turns off at higher negative gate voltage $V_{gs}$, compared to device A. An additional negative gate bias of about 8 V pinches off the transistor with initially 2.3 times higher 2DEG density. Correspondingly, the subthreshold drain current is higher in device B. The subthreshold gate current is $\sim 31\ \mu$A mm$^{-1}$ for device A and $\sim 60\ \mu$A mm$^{-1}$ for device B at drain voltage $V_{ds} = 13$ V, and the gate leakage seems to be the dominant factor for the subthreshold drain current in device A. However, a higher 2DEG density in sample B has been achieved due to lower In mole ratio ($x = 0.16$) in the $In_xAl_{1-x}N$ barrier layer; thus, lattice mismatch and tolerances of technological process cause worse interdevice insulation and contribute to higher subthreshold drain current of device B as well.

The best operation bias in terms of transconductance $g_m$ and self-heating is $I_d = 97$ mA mm$^{-1}$ at $V_{gs} = -2$ V for device A (figure 2), whereas $I_d = 146$ mA mm$^{-1}$ at $V_{gs} = -8$ V for device B (figure 3). Despite the different as-grown properties (initial 2DEG density, In mole ratio) the same peak value of $g_m \sim 145$ mS mm$^{-1}$ is observed at $V_{ds} = 13$ V for both devices A and B (figure 1, symbols). Certainly devices A and B have also close values of output conductance $g_D \sim 1$ mS mm$^{-1}$ at the optimum gate bias. The saturation knee of the output characteristics is at same $V_{ds} \sim 1$ V at the optimal gate bias points (figures 2–3, curves highlighted with arrows). A negative gate voltage controls the quantum wells' depth and the 2DEG density in the active part of the channel. The similar points of saturation current and similar values of $g_m$ and $g_D$ drives to the idea that the condition for the maximum

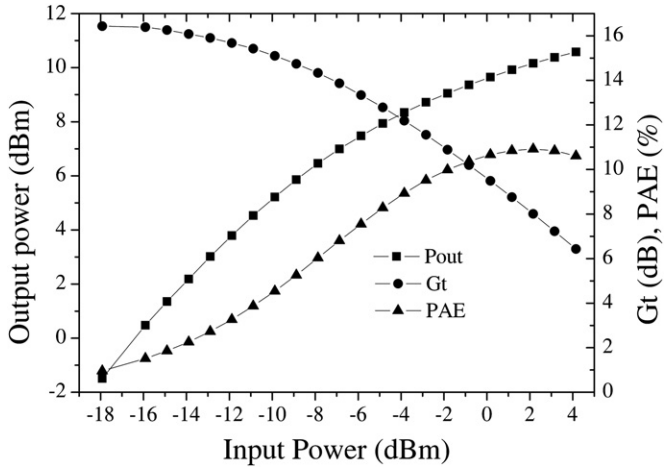


**Figure 4.** Output power versus input power for device A ($L_g = 2\ \mu$m, $W_g = 2\ \times\ 50\ \mu$m) at 4 GHz for $\Gamma_{\text{Source}} = (0.777; 0.365)$, $\Gamma_{\text{Load}} = (0.829; 0.117)$, $V_{\text{ds}} = 13$ V and $V_{\text{gs}} = -2$ V.

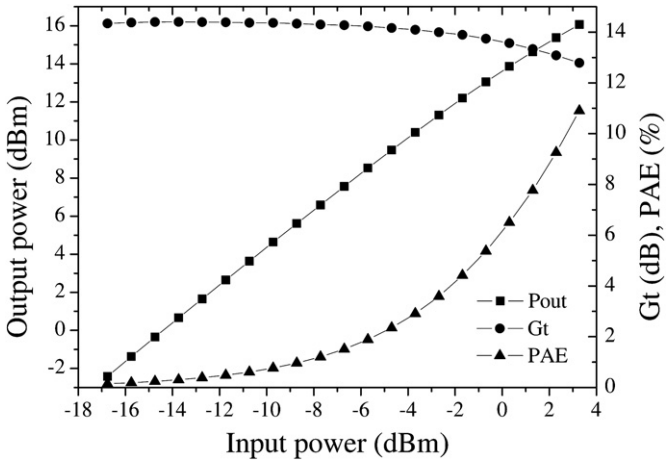


**Figure 5.** Output power versus input power for device B ($L_g = 2\ \mu$m, $W_g = 2\ \times\ 50\ \mu$m) at 4 GHz for $\Gamma_{\text{Source}} = (0.685; 0.500)$, $\Gamma_{\text{Load}} = (0.797; 0.195)$, $V_{\text{ds}} = 13$ V and $V_{\text{gs}} = -8$ V.

transconductance of the devices is at similar 2DEG density in the active part of the channel.

The power characteristics are measured for a matched source and load in the 1–8 GHz frequency range shown in figures 4–5, where $\Gamma_{\text{Source}}$ and $\Gamma_{\text{Load}}$ stand for the reflection coefficients for the source and load, respectively. The InAlN/AlN/GaN HFET with higher 2DEG density demonstrates more linear transducer power gain $G_t$ compared to HFET with lower 2DEG electron density (figures 4–5). Correspondingly, the gain compression starts at a lower input power in device A. Despite higher dc biasing and stronger subthreshold drain leakage current, device B (compared to device A) exhibits higher power gain and linearity of the output power with comparable power added efficiency (PAE), which is in favor of devices with higher 2DEG density.

Device B is set to the optimum operating condition at higher negative gate voltages (figures 1–3) compared to device A. Therefore, the extracted peak values of the cutoff frequency $f_T$ were obtained at the gate voltages ranging from $-8$ V to $-9$ V and from $-1.9$V to $-2.2$ V for series of devices

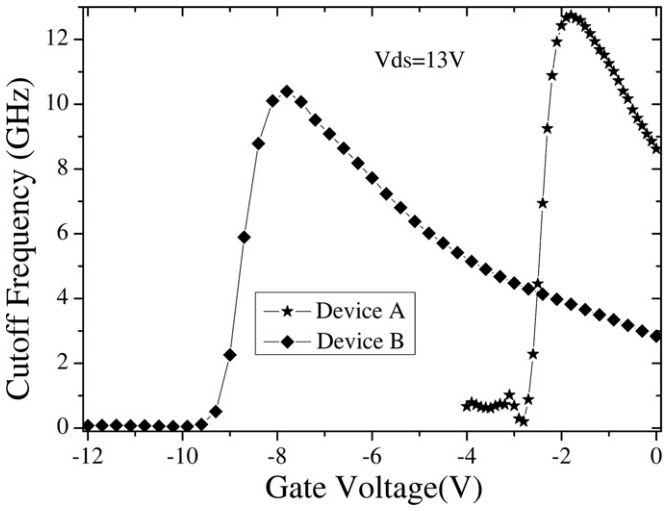


**Figure 6.** Current gain cutoff frequency versus $V_{\text{gs}}$ for devices A (stars) and B (diamonds) ($L_g = 2\ \mu$m, $W_g = 2\ \times\ 50\ \mu$m).

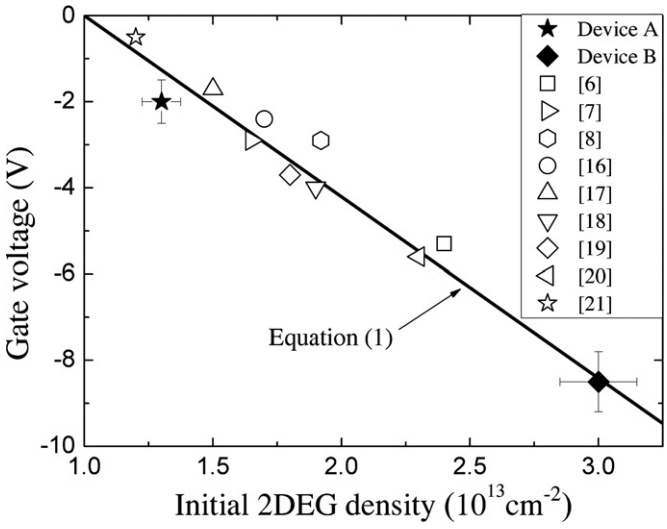


**Figure 7.** Optimal gate voltage dependence on initial 2DEG density of as-grown heterostructures for the fastest short-gate GaN HFETs (open symbols) and long-gate devices A (closed star) and B (closed diamond).

B and A, respectively (figure 6). The peak cutoff frequency exceeds 10 GHz for selected devices.

## 4. Discussion

Let us compare the optimal operation conditions for the investigated devices (figure 6) with those for the GaN HFETs with the record frequency performance, over 200 GHz [6–8, 16–21]. While the cutoff frequency depends on scaling down of a transistor and on parasitic elements, the optimal gate bias is mainly dependent on the as-grown 2DEG density (figure 7). In particular, the optimal gate voltage for device A (figure 7, solid star) is close to the open symbols for the deep submicron gate length HFETs. On the other hand, the diamond at $n_s = 3\ \times\ 10^{13}$ cm$^{-2}$ provides the result outside the range of the reported results [6–8, 16–21]. Nevertheless, the extrapolation of the best fit line (solid line) hits the result for

device B. Despite different cutoff frequencies, the optimal gate bias data for the long-gate (micron length) HFETs (figure 7, solid diamond and solid star) agree with those of the short-gate (deep submicron length) HFETs (open symbols).

The optimum gate voltage $V_g$ can be expressed via the gate effective capacitance per unit gate area $C_g$ and the active 2DEG density $n_g$ in the part of the channel controlled by the gate bias as follows:

$$V_g = \frac{(n_g - n_s) \times e}{C_g}, \quad (1)$$

where $n_s$ is the initial 2DEG density and $e$ is the elementary charge. The solid line (figure 7) is equation (1) drawn for $n_g = 1 \times 10^{13}$ cm$^{-2}$, $C_g = 3.8 \times 10^{-7}$ F cm$^{-2}$. The effective gate capacitance has a value close to that of the internal gate-source capacitance $C_{gs}$ in the small-signal model extracted from the two-port $Y$-parameters obtained through conversion of the de-embedded $s$-parameters for our devices. Comparable values for $C_{gs}$ in the range from $3.0 \times 10^{-7}$ F cm$^{-2}$ to $12 \times 10^{-7}$ F cm$^{-2}$ were reported for GaN HFETs [8, 22–26].

The optimum operating condition of the short-gate high-frequency HFETs and our relatively long-gate devices are located near the solid line in figure 7 defined by equation (1). Although this empirical relation between the optimum gate voltage and the 2DEG density assumes a simple parallel plate capacitor model and ignores realistic electric field distribution, it describes the experimental data for the short-gate and the long-gate HFETs in a universal way.

The extracted active 2DEG density, $n_g = 1 \times 10^{13}$ cm$^{-2}$, is close to the resonance 2DEG density associated with plasmon-assisted decay of hot phonons [14, 15]. The signatures of plasmons have been observed in different phenomena including HFET degradation, phase noise, electron drift velocity and transistor cutoff frequency [15].

## 5. Conclusion

The plasmon-controlled dependence of the optimum gate voltage on the 2DEG density is confirmed for 2 $\mu$m gate GaN HFETs in the range from $1.3 \times 10^{13}$ cm$^{-2}$ to $3 \times 10^{13}$ cm$^{-2}$. Despite a different gate length and initial 2DEG density in as-grown channels, the optimum gate voltage is predictable with the simple linear dependence (equation (1)) obtained from the plate capacitor model. In other words, the best operation is demonstrated at the same optimum electron density in the active part of the channel regardless of the initial 2DEG density and the gate length. The optimum active electron density is achieved through application of the optimum gate bias: the channels with higher 2DEG density require more negative voltage on the gate. The optimum active density of a GaN HFET coincides with that reported for the plasmon-controlled resonance known from independent experiments.

## Acknowledgments

This work is funded, in part, by the Research Council of Lithuania (grant MIP-056/2012) and the US Air Force Office of Scientific Research (grants FA8655-09-1-3103 and FA8655-12-1-2109). AŠ is thankful to this work foundation by European Union Structural Funds project 'Postdoctoral Fellowship Implementation in Lithuania' within the framework of the Measure for Enhancing Mobility of Scholars and Other Researchers and the Promotion of Student Research (VP1-3.1-ŠMM-01) of the Program of Human Resources Development Action Plan.

## References

[1] Morkoç H 2009 *Handbook of Nitride Semiconductors and Devices* vol 3 (Weinheim: Wiley-VCH)
[2] Shur M S and Maki P 2009 *Advanced High Speed Devices* (Singapore: World Scientific Publishing Company)
[3] Lu W, Kumar V, Schwindt R, Piner E and Adesida I 2002 DC, RF, and microwave noise performances of AlGaN/GaN HEMTs on sapphire substrates *IEEE Trans. Microw. Theory* **50** 2499–504
[4] Delage S L *et al* 2010 Achievement and perspective of GaN technology for microwave applications *18th Int. Conf. on Microwave Radar and Wireless Communications (MIKON) (Vilnius, Lithuania, 14–16 June 2010)* pp 1–5
[5] Rudolph M, Behtash R, Doerner R, Hirche K, Wurfl J, Heinrich W and Trankle G 2007 Analysis of the survivability of GaN low-noise amplifiers *IEEE Trans. Microw. Theory* **55** 37–43
[6] Haifeng Sun, Alt A R, Benedickter H, Feltin E, Carlin J–F, Gonschorek M, Grandjean N R and Bolognesi C R 2010 205-GHz (Al,In)N/GaN HEMTs *IEEE Electron Device Lett.* **31** 957–59
[7] Lee DS, Gao X, Guo S, Kopp D, Fay P and Palacios T 2011 300-GHz InAlN/GaN HEMTs with InGaN back barrier *IEEE Electron Device Lett.* **32** 1525–27
[8] Yuanzheng Yue *et al* 2012 InAlN/AlN/GaN HEMTs with regrown ohmic contacts and $f_T$ of 370 GHz *IEEE Electron Device Lett.* **33** 988–90
[9] Ikeda N, Niiyama Y, Kambayashi H, Sato Y, Nomura T, Kato S and Yoshida S 2010 GaN power transistors on Si substrates for switching applications *Proc. IEEE* **98** 1151–61
[10] Green B M 2009 *Advanced Semiconductor Materials and Devices Research: III-Nitrides and SiC* ed H-Y Cha (Kerala: Transworld Research Network) p 145
[11] Kuzmik J 2001 Power electronics on InAlN/(In)GaN: Prospect for a record performance *IEEE Electron Device Lett.* **22** 510–12
[12] Tasli P, Sarikavak B, Atmaca G, Elibol K, Kuloglu A F and Lisesivdin S B 2010 Numerical simulation of novel ultrathin barrier n-GaN/InAlN/AlN/GaN HEMT structures: effect of indium-mole fraction, doping and layer thicknesses *Physica* B **405** 4020–26
[13] Hiroki M, Yokoyama H, Watanabe N and Kobayashi T 2006 High-quality InAlN/GaN heterostructures grown by metal–organic vapor phase epitaxy *Superlattices Microstruct.* **40** 214–18
[14] Matulionis A, Liberis J, Matulioniene I, Ramonas M and Sermuksnis E 2010 Ultrafast removal of LO-mode heat from a GaN-based two-dimensional channel *Proc. IEEE* **98** 1118–26
[15] Matulionis A *et al* 2012 Window for better reliability of nitride heterostructure field effect transistors *Microelectron. Reliab.* **52** 2149–52
[16] Lee DS, Gao X, Guo S and Palacios T 2011 InAlN/GaN HEMTs with AlGaN back barriers *IEEE Electron Device Lett.* **32** 617–19
[17] Dong Seup Lee, Chung J W, Han Wang, Xiang Gao, Shiping Guo, Fay P and Palacios T 2011 245-GHz

InAlN/GaN HEMTs with oxygen plasma treatment *IEEE Electron Device Lett*. **32** 755–57

[18] Ronghua Wang, Guowang Li, Laboutin O, Yu Cao, Johnson W, Snider G, Fay P, Jena D and Huili Xing 2011 210-GHz InAlN/GaN HEMTs with dielectric-free passivation *IEEE Electron Device Lett*. **32** 892–94

[19] Ronghua Wang *et al* 2011 220-GHz quaternary barrier InAlGaN/AlN/GaN HEMTs *IEEE Electron Device Lett*. **32** 1215–17

[20] Tirelli S, Marti D, Haifeng Sun, Alt A R, Carlin J-F, Grandjean N and Bolognesi C R 2011 Fully passivated AlInN/GaN HEMTs with of 205/220 GHz *IEEE Electron Device Lett*. **32** 1364–66

[21] Shinohara K *et al* 2011 Deeply-scaled self-aligned-gate GaN DH-HEMTs with ultrahigh cutoff frequency *2011 IEEE Int. Electron Devices Meeting (Washington, DC, USA, 5–7 December 2011)* pp 19.1.1–19.1.4

[22] Chabak K D *et al* 2010 Full-wafer characterization of AlGaN/GaN HEMTs on free-standing CVD diamond substrates *IEEE Electron Device Lett*. **31** 99–101

[23] Chung J W, Hoke W E, Chumbes E M and Palacios T 2010 AlGaN/GaN HEMT with 300-GHz $f_{max}$ *IEEE Electron Device Lett*. **31** 195–97

[24] Shinohara K *et al* 2010 220 GHz fT and 400 GHz fmax in 40-nm GaN DH-HEMTs with re-grown ohmic *IEEE Int. Electron Devices Meeting (San Francisco, CA, USA, 6–8 December 2010)* pp 30.1.1–30.1.4

[25] Taking S, MacFarlane D, Khokhar A Z, Dabiran A M and Wasige E 2010 DC and RF performance of AlN/GaN MOS-HEMTs *2010 Asia-Pacific Microwave Conf. Proc. (Yokohama, Japan, 7–10 December 2010)* pp 445–48

[26] Shinohara K *et al* 2011 Electron velocity enhancement in laterally scaled GaN DH-HEMTs with fT of 260 GHz *IEEE Electron Device Lett*. **32** 1074–76